AGU PUBLICATIONS

Geophysical Research Letters

RESEARCH LETTER
10.1002/2015GL066645

Key Points:
- We made airborne observations of enhanced oxidized mercury and bromine monoxide
- The air mass subsided in the upper troposphere of the subtropical Pacific High
- Box modeling supports bromine-induced mercury oxidation in the free troposphere

Supporting Information:
- Supporting Information S1

Correspondence to:
L. E. Gratz,
lgratz@coloradocollege.edu

Citation:
Gratz, L. E., et al. (2015), Oxidation of mercury by bromine in the subtropical Pacific free troposphere, *Geophys. Res. Lett.*, *42*, doi:10.1002/2015GL066645.

Received 18 OCT 2015
Accepted 21 NOV 2015
Accepted article online 25 NOV 2015

Oxidation of mercury by bromine in the subtropical Pacific free troposphere

L. E. Gratz[1], J. L. Ambrose[2], D. A. Jaffe[3,4], V. Shah[4], L. Jaeglé[4], J. Stutz[5], J. Festa[5], M. Spolaor[5], C. Tsai[5], N. E. Selin[6], S. Song[6], X. Zhou[7,8], A. J. Weinheimer[9], D. J. Knapp[9], D. D. Montzka[9], F. M. Flocke[9], T. L. Campos[9], E. Apel[9], R. Hornbrook[9], N. J. Blake[10], S. Hall[9], G. S. Tyndall[9], M. Reeves[9], D. Stechman[9], and M. Stell[9]

[1]Environmental Program, Colorado College, Colorado Springs, Colorado, USA, [2]College of Engineering and Physical Sciences, University of New Hampshire, Durham, New Hampshire, USA, [3]School of Science, Technology, Engineering, and Mathematics, University of Washington Bothell, Bothell, Washington, USA, [4]Department of Atmospheric Sciences, University of Washington, Seattle, Washington, USA, [5]Department of Atmospheric and Oceanic Sciences, University of California, Los Angeles, California, USA, [6]Department of Earth, Atmospheric and Planetary Sciences, Massachusetts Institute of Technology, Cambridge, Massachusetts, USA, [7]Wadsworth Center, NYSDOH, Albany, New York, USA, [8]Department of Environmental Health Sciences, SUNY Albany, Albany, New York, USA, [9]National Center for Atmospheric Research, Boulder, Colorado, USA, [10]School of Physical Sciences, University of California, Irvine, California, USA

Abstract Mercury is a global toxin that can be introduced to ecosystems through atmospheric deposition. Mercury oxidation is thought to occur in the free troposphere by bromine radicals, but direct observational evidence for this process is currently unavailable. During the 2013 Nitrogen, Oxidants, Mercury and Aerosol Distributions, Sources and Sinks campaign, we measured enhanced oxidized mercury and bromine monoxide in a free tropospheric air mass over Texas. We use trace gas measurements, air mass back trajectories, and a chemical box model to confirm the origin and chemical history of the sampled air mass. We find the presence of elevated oxidized mercury to be consistent with oxidation of elemental mercury by bromine atoms in this subsiding upper tropospheric air mass within the subtropical Pacific High, where dry atmospheric conditions are conducive to oxidized mercury accumulation. Our results support the role of bromine as the dominant oxidant of mercury in the upper troposphere.

1. Introduction

Atmospheric chemistry and transport are fundamental in determining the introduction of mercury (Hg) to terrestrial and aquatic ecosystems. While gaseous elemental mercury (Hg(0)) may remain in the atmosphere for months, chemical conversion to the more soluble oxidized form facilitates atmospheric deposition [*Selin*, 2009; *Driscoll et al*., 2013]. Deciphering the mechanism for atmospheric Hg(0) oxidation is therefore critical to fully understanding the global Hg cycle.

Modeling studies suggest that atomic bromine (Br) is the primary global oxidant of Hg(0) [*Holmes et al*., 2006; *Holmes et al*., 2010; *Hynes et al*., 2009; *Shah et al*., 2015]. Although oxidation of Hg(0) by ozone (O_3) and the hydroxyl radical (OH) has also been proposed [*Calvert and Lindberg*, 2005], the gas-phase reactions of Hg(0) with these oxidants are probably too slow to be the dominant oxidation mechanism in the atmosphere [*Hynes et al*., 2009; *Subir et al*., 2011; *Driscoll et al*., 2013]. Bromine-initiated Hg(0) oxidation likely proceeds by a two-step mechanism, in which Hg(0) reacts with atomic Br to produce the unstable product HgBr that can either dissociate or react with other species (Br, OH, BrO, HO_2, or NO_2) to form inorganic oxidized Hg (Hg(II)) compounds [*Holmes et al*., 2010; *Goodsite et al*., 2004, 2012; *Dibble et al*., 2012, 2013]. The experimentally and theoretically determined reaction rate constants for this mechanism vary widely [*Subir et al*., 2011], creating one source of uncertainty around atmospheric Hg(0) oxidation and this mechanism's global relevance.

Another major limitation is the lack of observational data, specifically simultaneous observations of Hg species and Br radicals ($BrO_x = Br + BrO$) in the atmosphere [*Subir et al*., 2011]. In situ observations in the marine boundary layer (MBL) [*Sprovieri et al*., 2010], and during Hg depletion events over the Dead Sea [*Obrist et al*., 2011] and at polar sunrise [*Steffen et al*., 2008] provide evidence for Hg(0) oxidation by BrO_x, but it has been unclear how these observations extend to the midlatitudes or the middle to upper troposphere [*Subir et al*., 2011]. Chemical transport models (CTMs) suggest that Hg(0) oxidation by Br takes place predominantly in the

free troposphere [*Holmes et al.*, 2006, 2010; *Seigneur and Lohman*, 2008]. Yet the available high-elevation and airborne-speciated Hg observations [*Swartzendruber et al.*, 2006; *Fain et al.*, 2009; *Sheu et al.*, 2010; *Lyman and Jaffe*, 2012; *Timonen et al.*, 2013; *Brooks et al.*, 2014; *Weiss-Penzias et al.*, 2015] provide insufficient constraints on the sources and chemistry of Hg(II) in the global atmosphere due to the episodic nature of observed Hg(II) enhancements, the relatively small spatial scale of data coverage [*Shah et al.*, 2015], and concerns over measurement methods [*Jaffe et al.*, 2014].

To quantify the role of BrO_x in free tropospheric Hg(0) oxidation, we measured atmospheric Hg and BrO on board the National Science Foundation/National Center for Atmospheric Research (NSF/NCAR) C-130 aircraft during the 2013 Nitrogen, Oxidants, Mercury and Aerosol Distributions, Sources, and Sinks (NOMADSS) campaign over the central and eastern U.S. Overall during NOMADSS, Hg(II) concentrations were higher in the free troposphere (1–7 km above sea level (asl)) than in the continental or marine boundary layers (<1 km asl) [*Shah et al.*, 2015]. We report here the measurements obtained during Research Flight 6 (RF-06) on 19 June 2013 over Texas. Compared to other NOMADSS flights, RF-06 provides a unique opportunity to explicitly investigate free tropospheric Hg(0) oxidation in an isolated air mass in which both BrO and Hg(II) were above their respective detection limits.

2. Methods

2.1. Measurements

2.1.1. Mercury

We measured total Hg (THg) and Hg(0) at 2.5 min integrated sample frequency using the University of Washington's Detector for Oxidized Hg Species (DOHGS) [*Lyman and Jaffe*, 2012; *Ambrose et al.*, 2013; *Ambrose et al.*, 2015]. *Ambrose et al.* [2015] describe the DOHGS instrument and its application during NOMADSS in detail. In short, the DOHGS uses a dual-channel method in which sample air in the THg channel passes through a continuously heated pyrolyzer to convert all Hg(II) compounds to Hg(0); simultaneously, sample air in the Hg(0) channel passes through an Hg(II) scrubbing material such that only Hg(0) reaches the downstream analyzer. Mercury concentrations on both channels are quantified using Tekran® 2537B Hg vapor analyzers. Oxidized Hg is quantified by the difference between THg and Hg(0) measurements; thus, Hg(II) concentrations represent the sum of the gaseous and particle-bound forms. We sampled ambient air through a rear-facing heated perfluoroalkoxy (PFA) inlet connected to a heated PFA sample line [*Lyman and Jaffe*, 2012; *Ambrose et al.*, 2015]. The DOHGS aircraft inlet has a 50% particle cut size of 0.9 μm, and minimal wall losses of Hg(II) are anticipated due to partitioning into the gas phase within the heated PFA inlet [*Lyman and Jaffe*, 2012]. We performed calibrations on the ground and in-flight using a custom-built Hg(0) permeation source [*Lyman and Jaffe*, 2012]. The performance of the DOHGS with respect to Hg(II) recovery was also extensively quantified in the laboratory prior to NOMADSS [*Ambrose et al.*, 2015] and during previous aircraft and ground-based campaigns [*Lyman and Jaffe*, 2012; *Ambrose et al.*, 2013] using $HgBr_2$ and $HgCl_2$ as proxies for atmospheric Hg(II).

Mercury concentrations are reported in units of nanograms per standard cubic meter (ng m^{-3}; 0°C and 1 atm). Overall uncertainties are estimated as the sum in quadrature of the 1σ precision and the systematic uncertainty, both of which are described by *Ambrose et al.* [2015]. For RF-06, the overall uncertainties in THg and Hg(0) measurements are ±7% and ±8%, respectively. For Hg(II), the 1σ precision is determined as the maximum of 0.024 × [Hg(0)] and 0.025; the systematic uncertainty is the sum in quadrature of 0.047 × [Hg(II)] and 0.024 × [Hg(0)] [*Ambrose et al.*, 2015]. The 3σ limit of detection (LOD) for Hg(II) is 0.114 ng m^{-3}.

2.1.2. Bromine Monoxide

We quantified BrO mixing ratios using the UCLA's airborne limb-scanning Differential Optical Absorption Spectroscopy (Mini-DOAS) instrument [*Platt and Stutz*, 2008]. For this analysis, we used measurements in the limb (0°) of scattered solar radiation in the ultraviolet (300–380 nm) channel. We analyzed BrO using the DOAS technique with a wavelength range of 346.2–360.3 nm following the approach by *Aliwell et al.* [2002]. The results of DOAS retrievals are Differential Slant Column Densities (DSCD), which are the path-integrated trace gas concentrations along the optical path in the atmosphere, relative to a solar reference. To convert the BrO DSCD to mixing ratios, we employed the McArtim Monte Carlo Radiative Transfer Model (RTM) [*Deutschmann et al.*, 2011] constrained by in situ observations of meteorological parameters and aerosol properties on board the C-130. Model outputs of BrO are reported in parts per trillion by volume

(pptv) with 2σ LODs of 0.5–1 pptv. Additional details on the UCLA Mini-DOAS instrument, analysis of spectral retrievals, and application of the RTM are provided in the supporting information.

2.1.3. Other C-130 Measurements

We measured O_3 mixing ratios in parts per billion by volume (ppbv) using a fast-response chemiluminescence instrument [*Pollack et al*., 2012] at 1 s frequency with an uncertainty of 5%. Meteorological and state measurements on board the C-130 were also collected at 1 s frequency. Ozone and water vapor (WV) mixing ratios were averaged to 2.5 min intervals for comparison with DOHGS concentrations. Additional measurements from the C-130 used for the chemical box model (section 2.2.2), including nitrogen oxides (NO_x), carbon monoxide, methane, organic Br species (CH_2Br_2, $CHBr_3$, $CHBr_2Cl$, and $CHBrCl_2$), aerosol number concentration, and photolysis frequencies, are described in the supporting information. Details on instruments used on board the C-130 during NOMADSS are provided at https://www.eol.ucar.edu/content/nomadss-c-130-documentation.

2.2. Model Analyses

We use several tools to interpret the airborne observations, including backward air mass trajectories, a detailed chemical box model describing the processes during the air mass transport, and the GEOS-Chem global Hg model. These tools are described below.

2.2.1. HYSPLIT

We calculated 14 day air mass back trajectories using the Hybrid Single-Particle Lagrangian Integrated Trajectory (HYSPLIT) model [*Draxler and Hess*, 1998]. Meteorological inputs were derived from National Centers for Environmental Prediction's Global Data Assimilation System (GDAS) archived at 3 h intervals on a $1° \times 1°$ latitude-longitude grid and 23 vertical levels, each 25–50 hPa high.

2.2.2. Chemical Box Model

We ran the RCAT 8.2 1-D model [*Geyer and Stutz*, 2004; *Tsai et al*., 2014] as a box model by setting vertical exchange coefficients to very low values at a constant altitude of 7 km, effectively turning off vertical transport. We held temperature and pressure constant at 250 K and 367 hPa, corresponding to mean values along the 14 day HYSPLIT back trajectories. We first optimized the model performance for simulation of the observed BrO (Tables S1–S4 in the supporting information). Initial concentrations of trace gases, inorganic Br (Br_y), and organic Br were either iterated to match available C-130 measurements or were chosen to be consistent with values in the literature (Table S4) as follows. The initial condition for inorganic Br ($Br_y = Br + 2Br_2 + BrO + HBr + HOBr + BrONO_2 + BrNO_2 + BrCl$) was 6.9 pptv, which we adopted in agreement with available MBL measurements [*Pszenny et al*., 2004]. This led to an initial noontime BrO level on day 1 of around 1 ppt, not unlike observations reported by *Volkamer et al*. [2015]. For organic Br compounds measured on board the C-130, initial mixing ratios were iterated until the model output matched available measurements. A total organic bromine ($CH_3Br + CH_2Br_2 + CHBr_3 + CH_2BrCl + CHBr_2Cl + CHBrCl_2$) mixing ratio of 10.5 pptv was then used, which compared well to measurements and simulations reported by *Saiz-Lopez et al*. [2012]. The Br-specific reactions and photolysis rates are shown in Table S2. Aerosol surface area per volume of air was 0.5 $\mu m\ cm^{-3}$ based on aircraft observations by the Ultra-High Sensitivity Aerosol Spectrometer instrument. We utilized reactive uptake coefficients for H_2SO_4 solutions, assuming a sulfate background aerosol in the Pacific free troposphere, to describe heterogeneous aerosol chemistry. Bromine-specific uptake coefficients are shown in Table S3. Other initial trace gas inputs were iterated so that the model outputs matched the measurements on the C-130 within reasonable uncertainty (Table S4). Photolysis frequencies measured at solar noon by the High-performance Instrumented Airborne Platform for Environmental Research (HIAPER) Airborne Radiation Package (HARP) [*Petropavlovskikh et al*., 2007] were used to constrain the photolysis frequencies for the days prior to our observations. Other photolysis frequencies were adopted from *Landgraf and Crutzen* [1998] or calculated based on available absorption cross sections. The diurnal variation of photolysis rates was simulated using a sinusoidal behavior and the length of the day of our BrO and Hg(II) observations.

The reaction kinetics implemented for Hg(0) oxidation by atomic Br follow the GEOS-Chem Hg model described by *Shah et al*. [2015] as described in section 2.2.3. Although temperature and pressure were held constant in the model, we recognize that changes in atmospheric conditions during transport could influence the chemical mechanisms, especially given the temperature dependence of the Hg oxidation kinetics. We therefore performed sensitivity analyses at the minimum and maximum temperatures (239 K and 261 K) and pressures (299 hPa and 457 hPa) along the trajectory histories to determine a range of transport times required to produce the observed Hg(II) concentration.

2.2.3. GEOS-Chem

GEOS-Chem (www.geos-chem.org, model version v9-02) is a global three-dimensional CTM [*Bey et al.*, 2001] that includes an atmosphere-ocean-land Hg simulation [*Selin et al.*, 2008]. Assimilated meteorological inputs for GEOS-Chem are from the NASA Global Modeling and Assimilation Office's Goddard Earth Observing system (GEOS). We used a nested grid configuration [*Zhang et al.*, 2012] with a 4° latitude by 5° longitude global grid and a 0.25° × 0.3125° grid over North America, each with 47 vertical levels. Anthropogenic Hg emissions are taken from the Arctic Monitoring and Assessment Programme/United Nations Environment Programme (AMAP/UNEP) [*Arctic Monitoring and Assessment Programme/United Nations Environment Programme*, 2013] and U.S. EPA 2011 NEI [*Environmental Protection Agency*, 2014] inventories.

The GEOS-Chem global model for Hg is described in the literature [*Holmes et al.*, 2010; *Zhang et al.*, 2012; *Shah et al.*, 2015]. The oxidant concentrations (Br, OH, BrO, HO_2, and NO_2) were obtained from a model simulation with HO_x-NO_x-VOC-O_3-BrO_x tropospheric chemistry [*Bey et al.*, 2001; *Parrella et al.*, 2012]. Although GEOS-Chem does consider gas-to-particle partitioning of oxidized Hg [*Amos et al.*, 2012], for the purposes of our analyses we summed the modeled concentrations of gaseous and particulate oxidized Hg to generate a single Hg(II) model concentration for comparison with the Hg(II) measured by the DOHGS instrument.

In the GEOS-Chem global Hg model, and in the box model described above, we used the following oxidation mechanism for Hg(0):

$$\mathrm{Hg(0)} + \mathrm{Br} + M \rightarrow \mathrm{HgBr} + M \quad k_1 = 1.46 \times 10^{-32} \times \left(\frac{T}{298}\right)^{-1.86} \ \mathrm{cm^6\ molecule^{-2}\ s^{-1}} \tag{1}$$

$$\mathrm{HgBr} \xrightarrow{M} \mathrm{Hg(0)} + \mathrm{Br} \quad k_2 = 4.0 \times 10^{9} \times \exp\left(\frac{-7292}{T}\right) s^{-1} \tag{2}$$

$$\mathrm{HgBr} + X \rightarrow \mathrm{Hg(II)} \quad k_3 = 2.5 \times 10^{-10} \times \left(\frac{T}{298}\right)^{-0.57} \ \mathrm{cm^3\ molecule^{-1}\ s^{-1}} \quad (X = \mathrm{Br, OH, BrO, HO_2, NO_2}) \tag{3}$$

where T is the temperature (K). These rate constants were obtained from recent laboratory and theoretical calculations [*Goodsite et al.*, 2004, 2012; *Donohoue et al.*, 2006; *Dibble et al.*, 2012, 2013].

3. Results and Discussion

During RF-06, we sampled over Texas at an average cruising altitude of 7 km asl for more than 1.5 hours (Figures 1 and 2). This air mass was marked by very low average WV (0.2 g kg^{-1}) and O_3 (39 ppbv) mixing ratios (Figure 2). The low O_3 indicates that the air mass was not of stratospheric origin. The O_3 and WV altitude profiles indicate a clear transition when entering this air mass above approximately 5 km asl (Figure S1a), implying that little mixing had occurred and that the dry air mass at this altitude had been isolated from the influence of the lower troposphere for many days.

Consistent with our observations, HYSPLIT 14 day back trajectories show distinctly different transport patterns between the free tropospheric air mass at 7 km asl (Figure 3a) and the boundary layer air we sampled prior to our ascent (Figure S2). The free tropospheric air mass spent several days circulating and subsiding within the Pacific anticyclone at altitudes of 9–12 km asl before being advected toward North America, farther descending by 2–3 km asl (Figure 3a). Prior to this, the air mass was likely influenced by convection from the subtropical Pacific lower free troposphere and/or boundary layer, which is supported by the occurrence of a strong convective cloud region in the Intertropical Convergence Zone (ITCZ) (Figure 3b). In contrast, air in the boundary layer was influenced by a mix of southeasterly flow and transport over the continent at much lower altitudes (Figure S2).

This clear separation in air masses is reflected in the measured Hg concentrations (Figures 2a, S1, and S3) and BrO mixing ratios (Figure 2b). For example, THg concentrations inside the free tropospheric air mass (1.27 ± 0.06 ng m^{-3}) were considerably lower than concentrations in the boundary layer, likely due to the influence of continental Hg sources on the air at lower altitudes. Similarly, Hg(0) concentrations in the free tropospheric air mass (1.02 ± 0.08 ng m^{-3}) were lower than concentrations measured prior to our ascent, due in part to the overall lower THg levels but also due the formation of Hg(II) in the free tropospheric air mass. Oxidized Hg increased as we ascended to 7 km asl and was consistently elevated in the air mass (mean $\pm 1\sigma$:

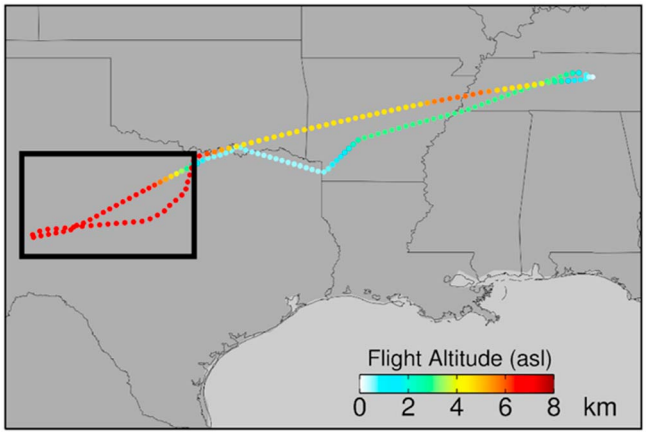

Figure 1. C-130 flight track for NOMADSS Research Flight 6 (RF-06) on 19 June 2013. The flight track color corresponds to the aircraft altitude in kilometers above sea level (km asl). The black box indicates the region where we observed the Hg(II)- and BrO-rich air mass.

0.266 ± 0.038 ng m^{-3}; range: 0.182–0.347 ng m^{-3}). Bromine monoxide was similarly below the detection limit in the boundary layer and increased to 1.9 ± 0.35 pptv inside the air mass during the ascent.

In summary, the chemical composition and back trajectories suggest a chemically aged air mass in the Texas free troposphere that was transported in the upper troposphere of the Pacific High over the previous approximately 2 weeks. The stable, dry conditions of large-scale anticyclones result in a lack of Hg(II) removal by wet deposition or in-cloud reduction and are thus ideal for Hg(II) accumulation. Additionally, the Hg(0) oxidation rate is presumably enhanced in the upper troposphere due to low temperatures that prevent thermal decomposition of the HgBr intermediate [*Holmes et al.*, 2010]. The transitions in WV and O_3 observed over Texas above ~5 km asl also indicate that this air mass did not experience much vertical mixing with surrounding air, providing a unique opportunity to investigate Br-induced Hg(0) oxidation.

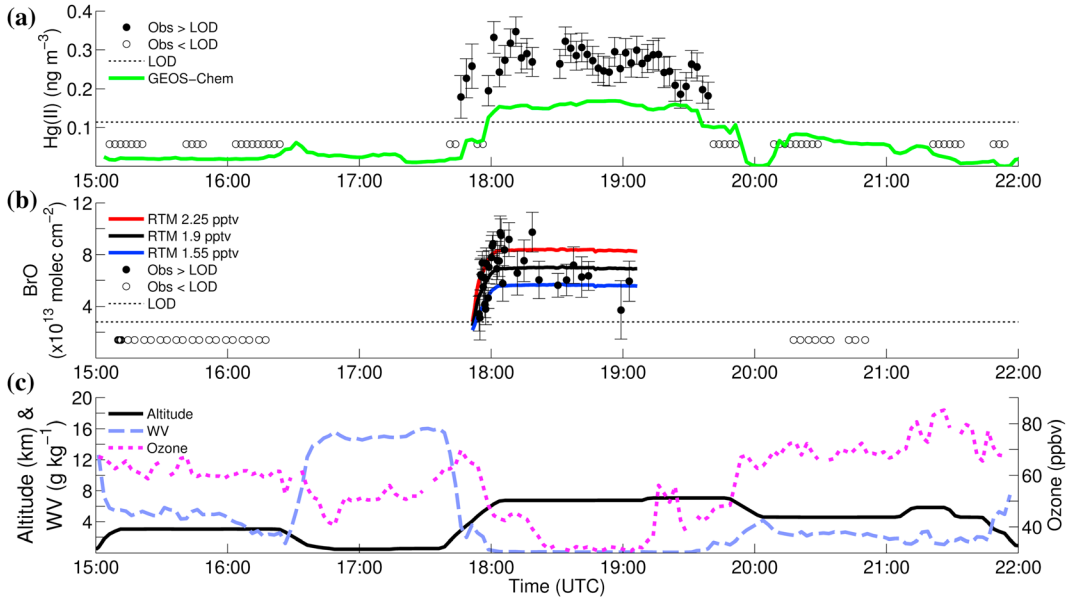

Figure 2. Observations from the NSF/NCAR C-130 during Research Flight 6 (RF-06) on 19 June 2013, when we sampled a dry free tropospheric air mass over Texas at a constant altitude of 7 km asl from 18:02:30 to 19:47:30 UTC. (a) Measured (black circles) and GEOS-Chem-modeled (green line) Hg(II) concentrations. Open circles represent Hg(II) concentration measurements below the limit of detection (LOD = 0.114 ng m^{-3} for RF-06); these measurements have been replaced with ½ LOD. Error bars represent the overall uncertainty in each Hg(II) measurement. (b) Bromine monoxide Differential Slant Column Densities (DSCD) measured during RF-06. Black dots represent the DOAS BrO DSCD with measurement errors shown as described in the supporting information. Measurements below the mini-DOAS LOD (2.8×10^{13} molecules cm^{-3}) have been replaced with ½ LOD. The blue, black, and red lines represent the DSCD calculated using the McArtim Radiative Transfer Model (RTM) for a 4 km wide BrO layer with mixing ratios of 1.55, 1.90, and 2.25 pptv centered at 7 km, respectively. (c) Flight altitude (solid black line), water vapor (WV) mixing ratios (dashed light blue line), and ozone (O_3) mixing ratios (dotted magenta line) during RF-06. Altitude, WV, and O_3 measurements are averaged to 2.5 min frequency corresponding to the Hg measurements.

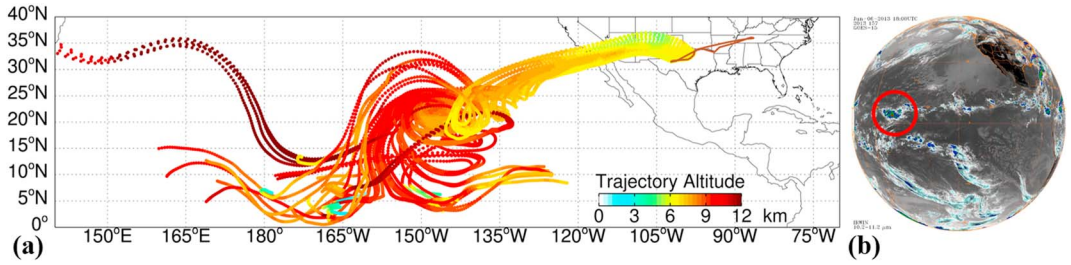

Figure 3. (a) HYSPLIT 14 day air mass back trajectories initiated every 2.5 min from 18:02:30 to 19:47:30 UTC along the C-130 flight track for NOMADSS RF-06 on 19 June 2013. The C-130 flight track is shown as a brown line. The color gradient of the trajectories corresponds to the trajectory altitudes (km asl). (b) GOES-15 IR satellite imagery (http://www.ncdc.noaa.gov/gibbs) on 6 June 2013 at 18:00 UTC (13 days prior to aircraft sampling over Texas during NOMADSS RF-06) showing strong convection in the ITCZ over the tropical Pacific Ocean. Colors in the satellite imagery correspond to cloud top altitudes.

We use the chemical box model to demonstrate that elevated BrO_x could persist and that sufficient Hg(II) could be produced during subsidence and long-range transport in the Pacific upper troposphere (Figure 4). The use of a box model is appropriate given the limited vertical mixing experienced by this air mass. By day 13 the model generates 1.9 pptv of BrO at 18:00–19:00 UTC (local solar noon) and the first hour of our measurement period. We find that the degradation of organic Br species provides a slow source of Br_y over the course of the simulation but cannot alone explain our BrO observations, and an initial Br_y source is needed. We speculate that this Br_y originated in the tropical Pacific MBL, where strong convection in the ITCZ lofted air into the free troposphere (Figure 3b). Such strong convection is common in the tropical Pacific and may be a source of halogen-rich air to the troposphere. We assume that precipitation desiccated the air mass as it ascended into the cold upper troposphere where, following the Hadley circulation, it was transported

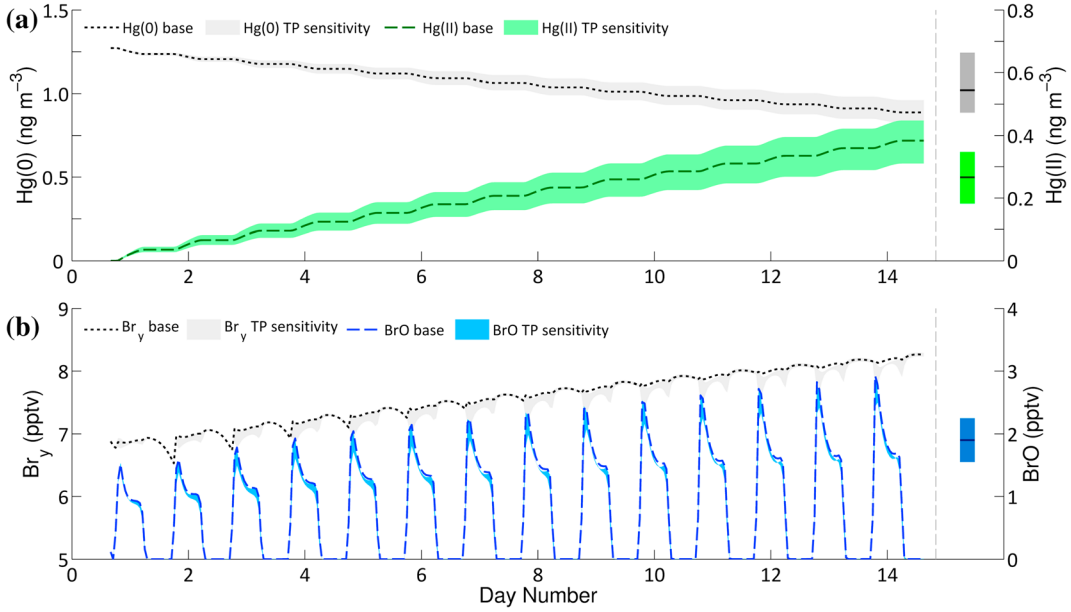

Figure 4. Hourly outputs from the chemical box model for (a) Hg(0) and Hg(II) and (b) Br_y and BrO. For comparison with the model output, vertical bars on the right-hand side of the plot show the mean and range of measured Hg(0) (gray), Hg(II) (green), and BrO (blue) in the free troposphere during RF-06; (mean values of 1.02 ng m^{-3} (Hg(0)), 0.266 ng m^{-3} (Hg(II)), and 1.9 pptv (BrO)). Major *x* axis tick marks for the box model output represent solar noon on each corresponding day of the simulation. Mixing ratios were calculated from the model concentrations using the air molecule concentration at the time of the C-130 observations to simplify comparison with our measurements; mixing ratios of Hg(0) and Hg(II) were then converted to ng m^{-3} at standard conditions of 0°C and 1 atm to match the observations (for Hg(0), 1 ng m^{-3} = 111.73 ppqv). Dashed lines represent results for each species from the base model run (T = 250 K and P = 367 hPa). Shading around each line represents the range of results from the temperature and pressure sensitivity simulations. Temperature and pressure in the "TP sensitivity" runs range from 239 K to 261 K and 299 hPa to 457 hPa, respectively.

northward to the subtropical Pacific High. However, because of uncertainty in the complex heterogeneous Br chemistry during convective uplift, we also acknowledge the alternative hypothesis that considerable Br_y may be present in the background tropical free troposphere [*Volkamer et al.*, 2015].

After optimizing the model performance for simulation of the observed BrO, we implemented the two-step mechanism for Hg(0) oxidation by atomic Br. We used an initial Hg(0) concentration of 1.27 ng m^{-3} (equivalent to the mean observed THg concentration) and an initial Hg(II) concentration of 0 ng m^{-3} to determine how much Hg(II) could be produced within the air mass during transport. We assumed conservation of THg throughout the simulation as follows. First, given the dry nature of the observed air mass, we neglected Hg(II) losses due to wet deposition or in-cloud reduction. This is supported by the back trajectory meteorological histories, which indicate that the mean transport time since the air mass over Texas encountered moderate rates of precipitation (>1 mm h^{-1}) was 11.8 days. Second, we neglected Hg removal by dry deposition assuming that the air mass was never in the boundary layer within the past 7–10 days. Finally, we ignored gas-to-particle Hg(II) partitioning given that the DOHGS Hg(II) measurements represent the sum of Hg(II) in both phases. These assumptions are consistent with the HYSPLIT back trajectories and our airborne observations.

We obtain the observed Hg(II) concentration on day 10 in the base model simulation, with 0.271 pg m^{-3} simulated at 18:00–19:00 UTC, while the sensitivity analyses suggest a range of 8 to 13 days required to produce the observed Hg(II) (Figure 4a). Over these same transport times the model also generates between 1.6 and 1.9 pptv of BrO at local solar noon (Figure 4b), confirming the ability for BrO_x to persist in the sampled air mass and thus for atomic Br to act as the dominant Hg(0) oxidant. These transport times are consistent with the back trajectories, and the box model results confirm the ability for Hg(II) to accumulate in the air mass in the absence of removal processes.

We use the GEOS-Chem output along the RF-06 flight track to determine whether the global model captures the observed Hg(II) enhancement. We find that model-simulated THg concentrations in the free tropospheric air mass (1.39 ± 0.01 ng m^{-3}; Figure S3) agree with our measured values; however, modeled Hg(II) concentrations (0.150 ± 0.019 ng m^{-3}) are significantly lower than the observations (Figure 2a). Thus, while GEOS-Chem correctly predicts the presence of an Hg(II)-rich air mass in the free troposphere over Texas, it substantially underestimates the magnitude of the enhancement. Notably, modeled BrO mixing ratios (0.40 pptv) are also significantly lower than measurements from the Texas free troposphere (1.9 pptv). One source of bias in the model oxidation mechanism is an underestimate in tropospheric BrO_x. Currently, modeled BrO_x in GEOS-Chem is based on best estimates for precursor emissions and up-to-date chemical mechanisms [*Parrella et al.*, 2012]. However, in the tropical free troposphere modeled BrO column densities are two to four times lower than satellite observations [*Parrella et al.*, 2012]. *Shah et al.* [2015] tested the impact of this bias on Hg oxidation in GEOS-Chem by tripling BrO_x in the subtropical free troposphere (45°S to 45°N and 750 hPa to the tropopause) and comparing the output with Hg(II) measurements from all NOMADSS flights. For RF-06, in the simulation with three times more BrO_x, Hg(II) concentrations (0.290 ± 0.063 ng m^{-3}) agree very closely with our observations. These results, together with our box model simulation, not only support the importance of the Br-oxidation mechanism in this region but demonstrate the need to better constrain the origins and levels of free tropospheric BrO_x in order to better understand the global Hg cycle.

Recognizing that uncertainties remain with respect to the potential role of other oxidants, we ran the base box model with Hg(0) oxidation by OH and O_3 (excluding the two-step Br oxidation mechanism) using rate constants reported by *Sommar et al.* [2001] and by *Hall* [1995] to be consistent with other modeling studies [*Selin et al.*, 2007, 2008; *Shah et al.*, 2015]. We find that Hg(0) oxidation by OH/O_3 alone only explains ~20% of the observed Hg(II) during RF-06 (Figure S4). *Shah et al.* [2015] also found that the OH/O_3 oxidation pathway in GEOS-Chem has only a minor impact on the Hg(II) generated in the upper troposphere. This is qualitatively in agreement with our observations showing higher THg and no detectable Hg(II) in the lower free troposphere for RF-06, despite the fact that O_3 mixing ratios were considerably higher there (Figures 2c and S1). *Shah et al.* [2015] additionally performed sensitivity tests to evaluate the GEOS-Chem response to a faster Hg(0) + Br oxidation rate constant and determined that, like in the aforementioned GEOS-Chem simulation with increased free tropospheric BrO_x, the model bias with respect to observations is significantly decreased. In other words, these two sensitivity tests by *Shah et al.* [2015] suggest that Hg(0) oxidation in the upper troposphere is substantially faster than in the base GEOS-Chem Hg model. However, given the enhanced

BrO measurements from RF-06, we attribute the GEOS-Chem model bias predominantly to an underestimate in the oxidant concentration. Considering our observations and the corresponding model analyses, we conclude that our results are consistent with Br as the dominant oxidant in the sampled air mass.

4. Conclusion

We report here an observational case study of significantly enhanced Hg(II) and BrO in the free troposphere, where much of the global oxidation of Hg(0) by Br is anticipated to take place. Using a box model that was optimized for observed BrO mixing ratios, we demonstrate that the observed Hg(II) can be reproduced by the two-step Br-initiated oxidation mechanism described by *Shah et al*. [2015]. Given the findings described here, we propose that Br is the main oxidant of Hg(0) in the subtropical free troposphere. We also propose that subtropical high-pressure systems are key locations in the global Hg cycle, where continuous large-scale subsidence and the absence of precipitation scavenging permits the presence of elevated BrO_x over extended periods and sustains Hg(II) accumulation. These unique meteorological conditions support the development of a large free tropospheric reservoir of Hg(II) that can be transported globally. Future measurements of Br_y and Hg(II) in the subtropical Pacific free troposphere would further elucidate the sources, sinks, and global budgets of these important atmospheric constituents.

Acknowledgments
The U.S. National Science Foundation provided funding for the NOMADSS project (awards 1217010 and 1215712). We thank the staff and scientists from the National Center for Atmospheric Research's Research Aviation Facility for their support throughout the study. Data from the NOMADSS campaign can be obtained through the Southeast Atmosphere Study home page (http://www.eol.ucar.edu/field_projects/sas).

References

Aliwell, S. R. et al. (2002), Analysis for BrO in zenith-sky spectra: An intercomparison exercise for analysis improvement. *J. Geophys. Res.*, *107*(D14), 4199 doi:10.1029/2001JD000329.

Arctic Monitoring and Assessment Programme/UNEP (2013), Technical background report for the global mercury assessment 2013. 263 (Arctic Monitoring and Assessment Programme/UNEP Chemicals Branch, Oslo, Norway/Geneva, Switzerland).

Ambrose, J. L., S. N. Lyman, J. Huang, M. S. Gustin, and D. A. Jaffe (2013), Fast time resolution oxidized mercury measurements during the Reno atmospheric Mercury Intercomparison Experiment (RAMIX), *Environ. Sci. Technol.*, *47*, 7285–7294, doi:10.1021/es303916v.

Ambrose, J. L., et al. (2015), Mercury emission ratios from coal-fired power plants in the southeastern United States during NOMADSS, *Environ. Sci. Technol.*, *49*, 10,389–10,397, doi:10.1021/acs.est.5b01755.

Amos, H. M., et al. (2012), Gas-particle partitioning of atmospheric Hg(II) and its effect on global mercury deposition, *Atmos. Chem. Phys.*, *12*, 591–603, doi:10.5194/acp-12-591-2012.

Bey, I., et al. (2001), Global modeling of tropospheric chemistry with assimilated meteorology: Model description and evaluation, *J. Geophys. Res.*, *106*, 23,073–23,095, doi:10.1029/2001JD000807.

Brooks, S., X. Ren, M. Cohen, W. T. Luke, P. Kelley, R. Artz, A. Hynes, W. Landing, and B. Martos (2014), Airborne vertical profiling of mercury speciation near Tullahoma, TN, USA, *Atmosphere*, *5*, 557–574, doi:10.3390/atmos5030557.

Calvert, J. G., and S. E. Lindberg (2005), Mechanisms of mercury removal by O_3 and OH in the atmosphere, *Atmos. Environ.*, *39*, 3355–3367, doi:10.1016/j.atmosenv.2005.01.055.

Deutschmann, T., et al. (2011), The Monte Carlo atmospheric radiative transfer model McArtim: Introduction and validation of Jacobians and 3D features, *J. Quant. Spectros. Radiat. Transfer*, *112*, 1119–1137, doi:10.1016/j.jqsrt.2010.12.009.

Dibble, T. S., M. J. Zelie, and H. Mao (2012), Thermodynamics of reactions of ClHg and BrHg radicals with atmospherically abundant free radicals, *Atmos. Chem. Phys.*, *12*, 10,271–10,279, doi:10.5194/acp-12-10271-2012.

Dibble, T. S., M. J. Zelie, and H. Mao (2013), Thermodynamics of reactions of ClHg and BrHg radicals with atmospherically abundant free radicals (vol 12, pg 10271, 2012), *Atmos. Chem. Phys.*, *13*, 9211–9212, doi:10.5194/acp-13-9211-2013.

Donohoue, D. L., D. Bauer, B. Cossairt, and A. J. Hynes (2006), Temperature and pressure dependent rate coefficients for the reaction of Hg with Br and the reaction of Br with Br: A pulsed laser photolysis-pulsed laser induced fluorescence study, *J. Phys. Chem. A*, *110*, 6623–6632, doi:10.1021/jp054688j.

Draxler, R. R., and G. D. Hess (1998), An overview of the HYSPLIT_4 modeling system of trajectories, dispersion, and deposition, *Aust. Meteorol. Mag.*, *47*, 295–308.

Driscoll, C. T., R. P. Mason, H. M. Chan, D. J. Jacob, and N. Pirrone (2013), Mercury as a global pollutant: Sources, pathways, and effects, *Environ. Sci. Technol.*, *47*, 4967–4983, doi:10.1021/es305071v.

Environmental Protection Agency (2014), *2011 National Emission Inventory, Version 1. Technical Support Document*, U.S. Environmental Protection Agency, Office of Air Quality Planning and Standards, Research Triangle Park, N. C.

Fain, X., D. Obrist, A. Hallar, I. Mccubbin, and T. Rahn (2009), High levels of reactive gaseous mercury observed at a high elevation research laboratory in the Rocky Mountains, *Atmos. Chem. Phys.*, *9*, 8049–8060, doi:10.5194/acp-9-8049-2009.

Geyer, A., and J. Stutz (2004), The vertical structure of OH-HO_2-RO_2 chemistry in the nocturnal boundary layer: A one-dimensional model study, *J. Geophys. Res.*, *109*, D16301, doi:10.1029/2003JD004425.

Goodsite, M. E., J. M. C. Plane, and H. Skov (2004), A theoretical study of the oxidation of Hg-0 to HgBr2 in the troposphere, *Environ. Sci. Technol.*, *38*, 1772–1776, doi:10.1021/es034680s.

Goodsite, M. E., J. M. C. Plane, and H. Skov (2012), A theoretical study of the oxidation of Hg0 to HgBr2 in the troposphere (vol 38, pg 1772, 2004), *Environ. Sci. Technol.*, *46*, 5262, doi:10.1021/es301201c.

Hall, B. (1995), The gas phase oxidation of elemental mercury by ozone, *Water Air Soil Pollut.*, *80*, 301–315, doi:10.1007/bf01189680.

Holmes, C. D., D. J. Jacob, and X. Yang (2006), Global lifetime of elemental mercury against oxidation by atomic bromine in the free troposphere, *Geophys. Res. Let.*, *33*, L20808, doi:10.1029/2006GL027176.

Holmes, C. D., D. J. Jacob, E. S. Corbitt, J. Mao, X. Yang, R. Talbot, and F. Slemr (2010), Global atmospheric model for mercury including oxidation by bromine atoms, *Atmos. Chem. Phys.*, *10*, 12,037–12,057, doi:10.5194/acp-10-12037-2010.

Hynes, A. J., D. L. Donohoue, M. E. Goodsite, and I. M. Hedgecock (2009), *Mercury Fate and Transport in the Global Atmosphere: Emissions, Measurements and Models*, edited by N. Pirrone and R. Mason, pp. 427–457, Springer, New York.

Jaffe, D. A., et al. (2014), Progress on understanding atmospheric mercury hampered by uncertain measurements, *Environ. Sci. Technol.*, *48*, 7204–7206, doi:10.1021/es5026432.
Landgraf, J., and P. J. Crutzen (1998), An efficient method for online calculations of photolysis and heating rates, *J. Atmos. Sci.*, *55*, 863–878, doi:10.1175/1520-0469.
Lyman, S. N., and D. A. Jaffe (2012), Formation and fate of oxidized mercury in the upper troposphere and lower stratosphere, *Nat. Geosci.*, *5*, 114–117, doi:10.1038/ngeo1353.
Obrist, D., E. Tas, M. Peleg, V. Matveev, X. Faïn, D. Asaf, and M. Luria (2011), Bromine-induced oxidation of mercury in the mid-latitude atmosphere, *Nat. Geosci.*, *4*, 22–26, doi:10.1038/ngeo1018.
Parrella, J. P., et al. (2012), Tropospheric bromine chemistry: Implications for present and pre-industrial ozone and mercury, *Atmos. Chem. Phys.*, *12*, 6723–6740, doi:10.5194/acp-12-6723-2012.
Petropavlovskikh, I., R. Shetter, S. Hall, K. Ullmann, and P. K. Bhartia (2007), Algorithm for the charge-coupled-device scanning actinic flux spectroradiometer ozone retrieval in support of the Aura satellite validation, *J. Appll. Remote Sens.*, *1*, doi:10.1117/1.2802563.
Platt, U., and J. Stutz (2008), *Differential Optical Absorption Spectroscopy: Principles and Applications*, Springer, Heidelberg.
Pollack, I. B., et al. (2012), Airborne and ground-based observations of a weekend effect in ozone, precursors, and oxidation products in the California South Coast Air Basin, *J. Geophys. Res.*, *117*, D00V05, doi:10.1029/2011JD016772.
Pszenny, A. A. P., J. Moldanová, W. C. Keene, R. Sander, J. R. Maben, M. Martinez, P. J. Crutzen, D. Perner, and R. G. Prinn (2004), Halogen cycling and aerosol pH in the Hawaiian marine boundary layer, *Atmos. Chem. Phys.*, *4*, 147–168.
Saiz-Lopez, A., et al. (2012), Estimating the climate significance of halogen-driven ozone loss in the tropical marine troposphere, *Atmos. Chem. Phys.*, *12*, 3939–3949, doi:10.5194/acp-12-3939-2012.
Seigneur, C., and K. Lohman (2008), Effect of bromine chemistry on the atmospheric mercury cycle, *J. Geophys. Res.*, *113*, D23309, doi:10.1029/2008JD010262.
Selin, N. E. (2009), Global biogeochemical cycling of mercury: A review, *Annu. Rev. Environ. Resour.*, *34*, 43–63, doi:10.1146/annurev.environ.051308.084314.
Selin, N. E., et al. (2007), Chemical cycling and deposition of atmospheric mercury: Global constraints from observations, *J. Geophys. Res.*, *112*, D02308, doi:10.1029/2006JD007450.
Selin, N. E., D. J. Jacob, R. M. Yantosca, S. Strode, L. Jaeglé, and E. M. Sunderland (2008), Global 3-D land-ocean-atmosphere model for mercury: Present-day versus preindustrial cycles and anthropogenic enrichment factors for deposition, *Global Biogeochem. Cycles*, *22*, GB2011, doi:10.1029/2007GB003040.
Shah, V., et al. (2015), Origin of oxidized mercury in the summertime free troposphere over the southeastern United States, *Atmos. Chem. Phys. Discuss.*, *15*, 26,839–26,893, doi:10.5194/acpd-15-26839-2015.
Sheu, G.-R., N.-H. Lin, J.-L. Wang, C.-T. Lee, C.-F. O. Yang, and S.-H. Wang (2010), Temporal distribution and potential sources of atmospheric mercury measured at a high-elevation background station in Taiwan, *Atmos. Environ.*, *44*, 2393–2400, doi:10.1016/j.atmosenv.2010.04.009.
Sommar, J., K. Gårdfeldt, D. Strömberg, and X. Feng (2001), A kinetic study of the gas-phase reaction between the hydroxyl radical and atomic mercury, *Atmos. Environ.*, *35*(17), 3049–3054, doi:10.1016/s1352-2310(01)00108-x.
Sprovieri, F., I. M. Hedgecock, and N. Pirrone (2010), An investigation of the origins of reactive gaseous mercury in the Mediterranean marine boundary layer, *Atmos. Chem. Phys.*, *10*, 3985–3997, doi:10.5194/acp-10-3985-2010.
Steffen, A., et al. (2008), A synthesis of atmospheric mercury depletion event chemistry in the atmosphere and snow, *Atmos. Chem. Phys.*, *8*, 1445–1482.
Subir, M., P. A. Ariya, and A. P. Dastoor (2011), A review of uncertainties in atmospheric modeling of mercury chemistry: I. Uncertainties in existing kinetic parameters—Fundamental limitations and the importance of heterogeneous chemistry, *Atmos. Environ.*, *45*, 5664–5676, doi:10.1016/j.atmosenv.2011.04.046.
Swartzendruber, P. C., et al. (2006), Observations of reactive gaseous mercury in the free troposphere at the Mount Bachelor Observatory, *J. Geophys. Res.*, *111*, D24302, doi:10.1029/2006JD007415.
Timonen, H., J. L. Ambrose, and D. A. Jaffe (2013), Oxidation of elemental Hg in anthropogenic and marine air masses, *Atmos. Chem. Phys.*, *13*, 2827–2836, doi:10.5194/acp-13-2827-2013.
Tsai, C., et al. (2014), Nocturnal loss of NO_x during the 2010 CalNex-LA study in the Los Angeles Basin, *J. Geophys. Res.-Atmos.*, *119*, 13,004–13,025, doi:10.1002/2014JD022171.
Volkamer, R., et al. (2015), Aircraft measurements of BrO, IO, glyoxal, NO_2, H_2O, O_2–O_2 and aerosol extinction profiles in the tropics: comparison with aircraft-/ship-based in situ and lidar measurements, *Atmos. Meas. Tech.*, *8*, 2121–2148, doi:10.5194/amt-8-2121-2015.
Weiss-Penzias, P., H. M. Amos, N. E. Selin, M. S. Gustin, D. A. Jaffe, D. Obrist, G.-R. Sheu, and A. Giang (2015), Use of a global model to understand speciated atmospheric mercury observations at five high-elevation sites, *Atmos. Chem. Phys.*, *15*, 1161–1173, doi:10.5194/acp-15-1161-2015.
Zhang, Y., et al. (2012), Nested-grid simulation of mercury over North America, *Atmos. Chem. Phys.*, *12*, 6095–6111, doi:10.5194/acp-12-6095-2012.